ACS OMEGA

Article

Cite This: ACS Omega 2018, 3, 8874−8881

http://pubs.acs.org/journal/acsodf

Lepidocrocite-Type Titanate Formation from Isostructural Prestructures under Hydrothermal Reactions: Observation by Synchrotron X-ray Total Scattering Analyses

Satoshi Tominaka,*[,†,‡] Hiroki Yamada,[§,‡] Satoshi Hiroi,[∥,‡] Saori I. Kawaguchi,[‡] and Koji Ohara[‡]

[†]International Center for Materials Nanoarchitectonics (WPI-MANA), National Institute for Materials Science (NIMS), 1-1 Namiki, Tsukuba, Ibaraki 305-0044, Japan

[‡]Research and Utilization Division, Japan Synchrotron Radiation Research Institute, 1-1-1 Kouto, Sayo-gun, Hyogo 679-5198, Japan

[§]Department of Chemical System Engineering, The University of Tokyo, 7-3-1 Hongo, Bunkyo, Tokyo 113-8656, Japan

[∥]Synchrotron X-ray Station at SPring-8, Research Network and Facility Services Division, National Institute for Materials Science (NIMS), 1-1-1 Koto, Sayo, Hyogo 679-5148, Japan

Supporting Information

ABSTRACT: The formation of titanium dioxides, such as rutile and anatase, is known to proceed through the formation of a lepidocrocite-type layered structure under hydrothermal conditions, but the nucleation of this intermediate is still not understood well. Here, the nucleation of lepidocrocite-type layered titanates under hydrothermal conditions is observed by tracking the structural changes by in situ time-resolved pair distribution function analyses. We found that titanate clusters or corrugated layered prestructures having <1 nm domains with lepidocrocite-type connectivity were formed even before thermal treatment in alkaline aqueous solution. Upon thermal treatment, a two-dimensional layered structure grew directly from the prestructure, not from the amorphous polymeric hydroxide dissolved in the solution. Thus, we conclude that the formation of the lepidocrocite-like prestructure is the key for forming a layered titanate under hydrothermal conditions.

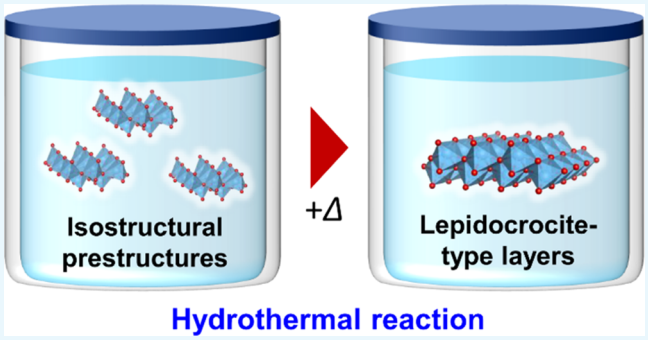

INTRODUCTION

Titanium dioxides, such as anatase and rutile, are widely used because of their low environmental impact and abundant resources. In the chemical formation of titanium dioxides, an intermediate lepidocrocite-type layered titanate often forms,[1−3] but other intermediates have also been observed under similar hydrothermal conditions.[2,4] Better understanding of the nucleation/growth mechanism is of great importance for titanite synthesis. However, more details, such as the nucleation of the intermediates from precursor solutions, remain to be clarified. Nucleation, an initiation step for forming a new phase having a low free energy from a phase having a higher energy, has been studied for decades, but a fundamental understanding has still not been attained. Classical nucleation theory provides a rough understanding of direct nucleation driven by thermal fluctuations, whereas other mechanisms, including the formation of intermediate clusters, often more accurately describe the phenomena.[5,6] The overall processes are complicated; hence, a variety of mechanisms might exist in reality. In particular, greater understanding of the nucleation of solid products in solvents during chemical reactions, which proceeds via the cleavage and formation of chemical bonds in precursor compounds, is required.

To clarify the process of nucleation in chemical synthesis, in situ time-resolved analysis techniques, using energy/angular-dispersive X-ray diffraction (XRD),[7−14] an X-ray pair distribution function (PDF) analysis,[4,15−17] and modified transmission electron microscopy (TEM),[18,19] can be used. XRD is advantageous for determining the kinetics of crystallization processes,[20,21] a PDF analysis is useful for clarifying the structural changes during nucleation and initial growth,[6] and TEM can track individual particles. In particular, monitoring the trajectory of formation of products is informative when examining nucleation. These in situ observations can remove the effect of recovery processes, including quenching, rinsing, and drying.

We observed the nucleation of titanates, particularly the nucleation and growth of the lepidocrocite-type structure, under hydrothermal conditions by in situ X-ray total scattering analyses. In the total scattering data, Bragg peaks clarify the

Received: July 18, 2018
Accepted: July 27, 2018
Published: August 9, 2018

DOI: 10.1021/acsomega.8b01693
ACS Omega 2018, 3, 8874−8881

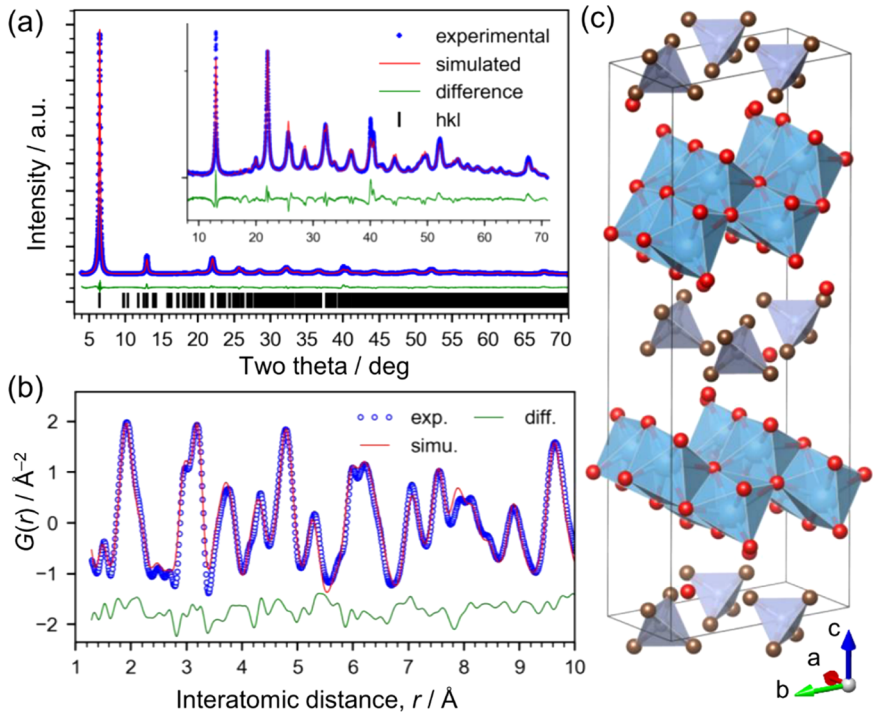

Figure 1. Ex situ X-ray structural analysis of the layered titanate crystals. (a) Rietveld refinement of XRD pattern (λ = 1.29945 Å). (b) PDF fitting (λ = 0.1076 Å, Q = 1.6–29.0 Å^{-1}). (c) Crystal structure model of the dried product, I (blue: Ti, red: O, gray: C, tetrahedra: C_4N).

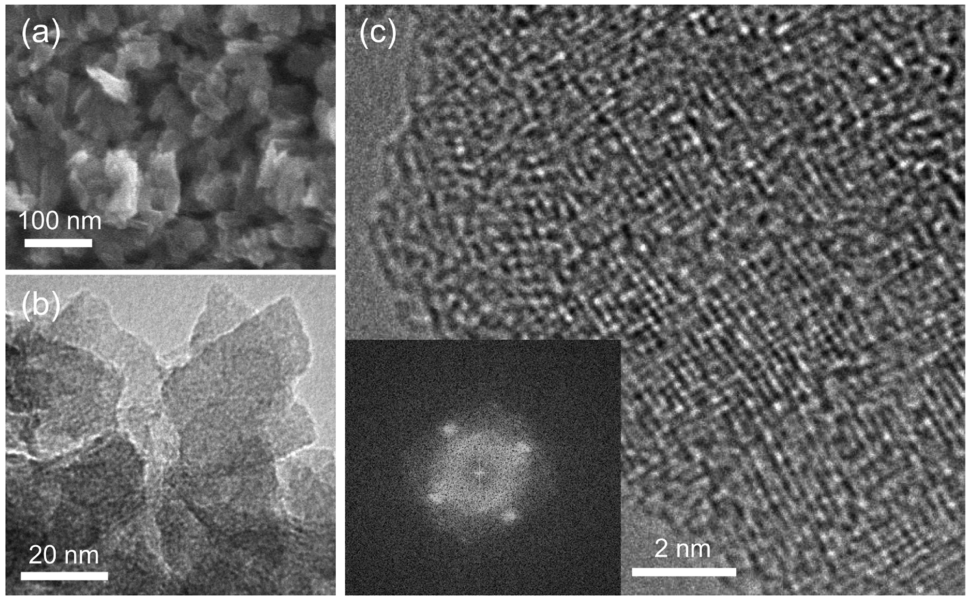

Figure 2. Electron microscope images of the lepidocrocite-type titanate powder. (a) SEM image. (b) TEM image. (c) High-resolution TEM image of a domain observed along the vertical direction of a planar particle. The inset shows a fast Fourier transform pattern, which exhibits rectangular symmetry.

growth of crystalline products and PDFs reveal local-to-medium-range structural transformations, particularly in the nucleation stage. PDFs are useful for determining the structures of crystalline, nanocrystalline, and amorphous materials.[14−16,22,23] They provide the distances and densities of atomic pairs ranging from coordination spheres (obtained by X-ray absorption fine structure (XAFS) analysis) to crystal structures. Thus, we investigated the structural changes of titanium oxides under hydrothermal conditions by analyzing in situ X-ray total scattering data.

RESULTS AND DISCUSSION

First, we analyzed the final product formed by the hydrothermal reaction of titanium isopropoxide in aqueous solution containing tetramethyl ammonium hydroxide (TMAH). After the reaction at 160 °C under microwave heating, the product was recovered from the solution and crystallized by a purification procedure (details in the Materials and Methods). Its composition was carefully determined as $[TiO_2]\cdot nH_2O\cdot m((CH_3)_4N)$ (n = 0.54 and m = 0.22) by elemental and

DOI: 10.1021/acsomega.8b01693
ACS Omega 2018, 3, 8874−8881

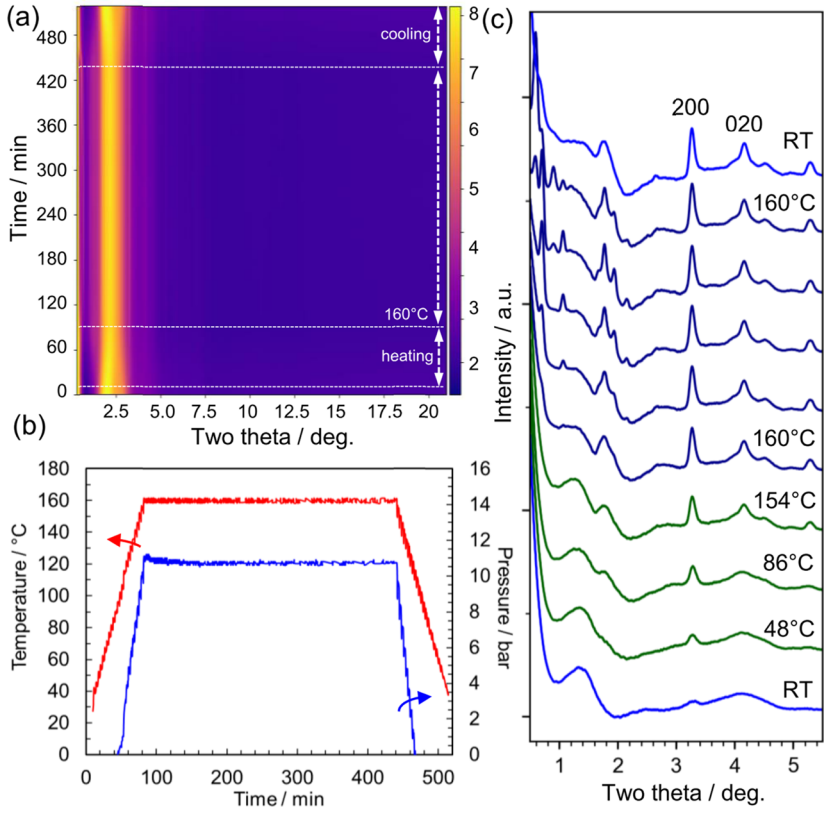

Figure 3. In situ X-ray total scattering measurements performed to investigate nucleation of titanate under hydrothermal conditions. (a) Two-dimensional (2D) data of time-dependent total scattering data (λ = 0.10790 Å). The scattering from the glass vial and air background was subtracted. The sample was kept at RT for 10 min and then heated up to 160 °C (VT). (b) Temperature and pressure measured during the X-ray experiments. (c) Selected profiles of the scattering data recorded at different times (RT: 0 min; 48 °C: 19 min; 86 °C: 39 min; 154 °C: 78 min; 160 °C: 100, 119, 159, 319, and 419 min; RT: 517 min from bottom to top). The solvent scattering data at the same temperature were subtracted. The *hkl* values, 200 and 020, are based on the structure model of the crystalline product analyzed at room temperature.

thermogravimetric analyses (Figure S1) and from the infrared spectrum (Figure S2).

The structure was determined by XRD (Figure 1a) and using the PDF (Figure 1b). The particles have a uniform size on the order of 10 nm (Figure 2). The PDF data, particularly the relative intensity of the peaks around 3.0 Å (assigned to the Ti−Ti distance in edge-shared TiO_6 octahedra) and 3.7 Å (assigned to the Ti−Ti distance in corner-shared TiO_6 octahedra), suggest that the structure is a lepidocrocite-type titanate.[1,3] The individual layers of the lepidocrocite-type titanate have orthorhombic symmetry, which we confirmed from the result of high-resolution TEM (Figure 2c). A titanate with a lepidocrocite-type structure is known to crystallize in isomorphous compounds with orthorhombic crystal structures having interlayer alkali-metal cations,[24,25] and thus we compared the experimental XRD pattern with simulated patterns, such as those of lepidocrocite titanate crystals of $K_{0.8}Ti_{1.73}Li_{0.27}O_4$ (KTLO) and $H_{1.07}Ti_{1.73}O_4$ (HTO), using the structure information available in the literature.[14] As shown in Figure S3, the XRD pattern for HTO is similar but not a close match to our data. This is reasonable because our material contains TMAH molecules. Since there is no reported crystal structure for lepidocrocite titanate with TMAH, we solved the structure and refined it by the Rietveld method, as described in the next paragraph.

As is often the case, we attempted to solve the structure by the direct method using the EXPO2014 program[26] but were unsuccessful. Then, we employed the real-space method using an initial structure model prepared by modifying the HTO-layered titanate structure.[14] We performed cycles of structure modification and refinement using the Rietveld method while checking the Fourier map showing the difference between the model and the electron density map calculated from the XRD data. As a result, the space group was determined to be *P*2, then the structure was further refined by the Rietveld method (Figure 1a). The symmetry is lower than that of the typical orthorhombic unit cell for lepidocrocite-type titanate[27] because of the presence of tetrahedral TMAH molecules rather than alkali-metal cations, such as K^+. The resultant structure is monoclinic (a = 5.939 Å, b = 7.588 Å, c = 23.651 Å, β = 103.857°, R_{wp} = 5.520, goodness-of-fit (GOF) = 0.727; structural information is available in the Supporting Information). The GOF value of less than 1.0 is considered to originate from the weak scattering at high angles causing a low R_{exp} value (7.593), and the fit itself is reasonably good. The mismatch found at high angles is probably due to the model based only on isotropic particle size because the integrated intensity for each peak appears to match that of experimental data well. Since the aim of this data analysis of the crystalline product is to determine the atomic arrangement in detail, we used PDF analysis for the further structural refinement, where the particle size effects are less dominant. The local structure of the titanate was investigated through PDF refinement (Figures 1b and S4) using the PDFfit2 program[28] (a = 5.944 (7) Å, b = 7.576 (9) Å, c = 23.56 (5) Å, β = 103.33° (16), R_w = 23.7%, fitting range = 1−30 Å; structural information is available in

DOI: 10.1021/acsomega.8b01693
ACS Omega 2018, 3, 8874−8881

the Supporting Information) and is illustrated in Figure 1c. Note that the coordinates of TMAH molecules were fixed to the positions refined by the XRD analysis because their contribution to the PDF was not significant, as shown in Figure S4b. The crystal structure consists of two layers of lepidocrocite-type titanate with interlayer water and TMAH molecules. We clarified that the reaction formed a lepidocrocite-type layered titanate.

As discussed above, we clarified that the reaction yielded a lepidocrocite-type layered titanate from the precursor solution. Next, we analyzed the reaction route by in situ time-resolved X-ray total scattering experiments. Figure 3 shows the time-resolved in situ X-ray total scattering used to investigate structural transformation proceeding under hydrothermal conditions. The solution was homogeneously heated from room temperature (RT) to 160 °C (5 °C steps and 5 min per step holding time) using microwave (Figures 3b and S5). Since the intense peak around 2.5° is mostly associated with the solvent molecules, we subtracted it using the data for the solution without titanate (Figure S6), and thus obtained Figure 3c, which clearly illustrates the growth of Bragg peaks. The peak at 3.28° grows even at 48 °C, and other peaks (e.g., 4.07°) appear at higher temperatures. Note that these two peaks are assigned to the in-plane diffraction peaks of the layered titanate structure (cf. Figures 1 and 4c).

During the thermal treatment at 160 °C, these peaks grew and other peaks assigned to out-of-plane diffraction appeared at lower angles. In particular, the peaks below 0.7°, assigned to stacking direction (the *c* axis in Figure 1c), shifted from 0.7 to 0.59°, which is close to the angle of 0.54° (002 diffraction from the crystalline product at RT, Figure 1). These results indicate that the stacking of layers proceeds. The solution changed from translucent to white during holding at 160 °C, but the solution became translucent again when cooled (Figure S7). This observation is consistent with the diffraction pattern (top, Figure 3c), which only contains in-plane diffraction peaks at low temperatures. This fact indicates lower solubility of the layered titanite at elevated temperatures, indicating negative entropy for the dissolution of the compound in water, which may be due to strong hydration of the layered titanate or TMAH molecules, as is known for $Ca(OH)_2$ and Li_2CO_3.

The in situ XRD data suggest the formation and growth of the layered titanate structure even during the period when the temperature was increased from RT to 160 °C (in ~80 min). To acquire further understanding of this process, the scattering data were converted into PDFs by a Fourier transform, where the solvent signal was subtracted, as shown in Figure 3c. We calculated the PDFs for the titanate compounds after subtracting the intensity of the solvent measured at the same temperature (Figure 4). The solvent contained water molecules and TMAH as well as isopropanol formed from titanium isopropoxide. The titanate species were removed before adding TMAH. Thus, the total scattering data from this solution can be regarded as identical to that from the solvent phase in the sample solution. Since the titanate forms solid-state structures, this subtraction is considered to remove the solvent signal effectively, as reported for nanoparticles.[29] Figure 4a shows the time dependence of the reduced PDF during the hydrothermal reaction. The peak positions are almost constant and identical to those of the lepidocrocite structure (Figure 4b). The structure within 20 Å did not significantly change, except in the initial 15 min, where the as-prepared sample grew abruptly after starting the thermal treatment at 10 min. The

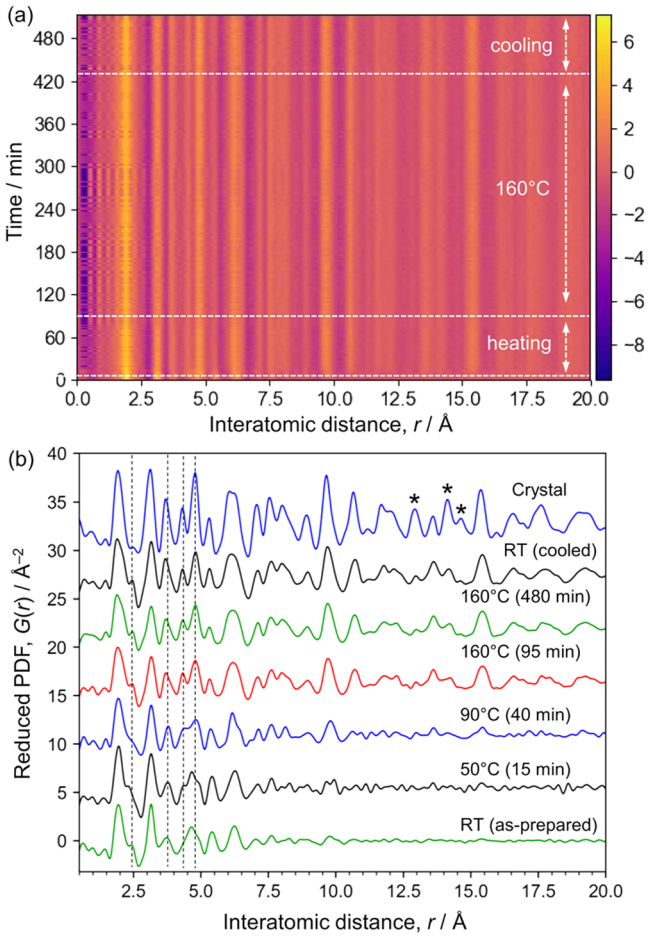

Figure 4. Time-dependent PDF data. (a) Two-dimensional plot of time-dependent in situ PDFs. (b) Selected one-dimensional plots shown with the ex situ PDF for the crystalline product. The total scattering intensity from the solvent was subtracted and then the remaining intensity was converted into PDFs. Ten frames (or 10 min) of data were integrated for the RT data and the data obtained at 160 °C (85–95 and 470–480 min). One frame of data was used for 50 and 90 °C. The same *Q* range (2.0–18.9 $Å^{-1}$) was used for the Fourier transform except that for the crystalline sample (1.6–18.9 $Å^{-1}$).

relative PDF data show this change more clearly, as shown in Figure S8 (details are available in the Supporting Information). This is consistent with the XRD results and no additional phase was found; thus, the structural change proceeds without forming an intermediate structure, that is, the structure transformation is direct.

The lepidocrocite structure grown after the thermal treatment (e.g., "RT (cooled)" in Figure 4b) has a PDF peak assigned to Ti–Ti pairs in edge-shared TiO_6 octahedra around 3.0 Å and one assigned to Ti–Ti pairs in corner-shared TiO_6 octahedra around 3.5 Å.[3] Consistent with the crystalline product, the relative intensities of these peaks indicate the formation of lepidocrocite layers, which have more edge-sharing TiO_6 octahedra than anatase, brookite, and rutile.[3] The PDF peak around 1.4 Å is too short for Ti–O bonds[30] and is assigned to the C–N distance in TMAH and probably to a termination ripple. Note that a peak corresponding to Ti═O double bonds may be observable around 1.6 Å,[31] but the absence of a peak in the infrared spectrum around 1000 cm^{-1}

DOI: 10.1021/acsomega.8b01693
ACS Omega 2018, 3, 8874–8881

rules out the formation of double bonds (Figure S9). The peak at 1.95 Å is assigned to Ti−O nearest neighbors.

The PDF was analyzed by curve fitting using an isolated nanosheet model, as shown in Figures 5 and S10, where an

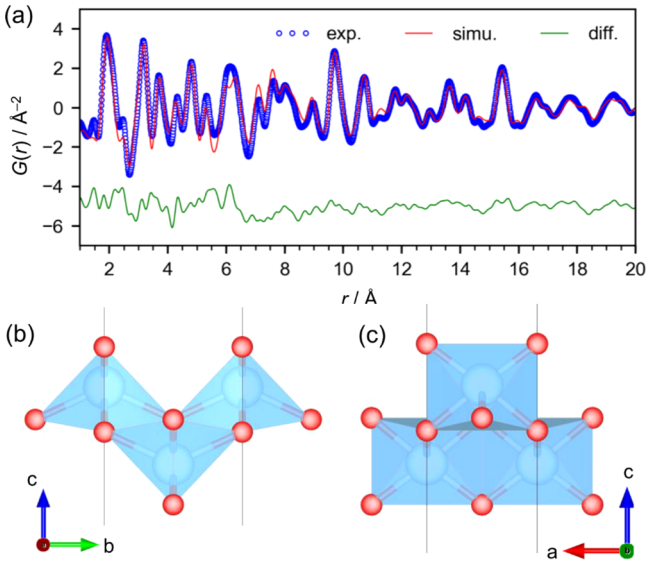

Figure 5. (a) PDF curve fitting result for the titanate in the heated solution measured at RT. (b, c) Lepidocrocite-type layered titanate structure model.

orthorhombic unit cell in the *Pmmn* space group was used (a = 2.987 (3) Å, b = 3.803 (3) Å, c = 100 Å, R_w = 16.5% in the range from 1 to 20 Å; the large c value was used to simulate the isolated structure; two Ti sites and four O sites). The lattice constants a and b are almost half of those of the crystalline product shown in Figure 1c, where the interlayer TMAH molecules lower the symmetry of the crystal structure. Note that we did not include the interlayer TMAH molecules found in the crystalline products because their contribution was not significant even in the crystalline product although they were considered to exist around the titanate layers. Thus, the model does not simulate the peak at 1.4 Å, which is assigned to C−N distance though it might be a termination ripple of the Fourier transform. Moreover, the model has an empty space along the c axis to simulate in-plane atomic correlation only using PDFfit2, but this model cannot properly simulate the background of the PDF, which reflects averaged number density of atoms. Thus, we simulated background of the PDF separately as shown in Figure S10, subtracted it from the experimental PDF, and then performed the curve fitting using PDFfit2.

Looking closely at the PDF of the titanate in the as-prepared solution, we found that the peak positions were slightly different from those in the grown lepidocrocite-layered titanate. First, there are no peaks above 7 Å (Figure 4b), meaning that the structure is tiny or highly corrugated. We simulated the PDFs of these typical TiO_2 crystals and layered hydroxide crystals ($H_2Ti_2O_3$, $H_2Ti_3O_7$, and lepidocrocite-type TiO_2) as shown in Figure S11. It is apparent that the Ti−Ti pairs in corner-shared TiO_6 octahedra are richer in the titanate in the as-prepared solution than those in typical TiO_2 crystals of anatase, rutile, and brookite. We confirmed that the lepidocrocite-type TiO_2 PDF most closely matched the experimental PDF (Figure S11f). The experimental PDF was fitted with the lepidocrocite structure with the highest symmetry (*Pmmn* space group; a = 3.040(8), b = 3.833(12) Å, c = 100 Å, R_w = 27.7% in the range from 1 to 15 Å) using the PDFfit2 program (Figure S10b).[28] There is an obvious mismatch between the experimental and simulated PDFs, suggesting that there are short-range chemical orders. For example, the titanate has a peak located around 3.7 Å (assigned to Ti−Ti in corner-shared octahedra), which is at a longer distance and broader than that in the typical lepidocrocite structure, whereas the peak at 4.9 Å (assigned to Ti−Ti along the diagonal direction) is at a shorter distance.

For the further analysis of the PDF data, we used a 2 × 2 × 1 supercell of the model (*P*1 space group; 8 Ti sites and 16 O sites). Performing the fitting with PDFfit2[28] for the 24 atoms in the *P*1 space group can collapse the structure during the least-squares fitting of the atomic coordinates, and thus we used our own program to modify the atomic coordinates through the random movement of one atom within a distance of 0.1 Å under the structural restraints of the bond lengths (Ti−O: 1.8−2.6 Å; Ti−Ti: >2.8 Å). We used PDFfit2 to simulate the PDF based on the structural model with fixed coordinates, and then we judged the acceptance or rejection of the structure modification on the basis of the R value exported from PDFfit2. Performing these cycles of structure modification and evaluation of the curve fitting is a type of reverse Monte Carlo simulation using a large-scale structure model. This can also be considered as the simulated annealing method, which is often used in XRD analysis because of the use of a structure model of a unit cell.[32] Since the surface O atoms coordinate to only two Ti atoms and thus are considered not to be well restrained by the data, we fixed their coordinates. This model can effectively simulate the experimental PDF (*P*1 space group; a = 6.169(13), b = 7.68(2) Å, c = 100 Å, R_w = 16.1% in the range from 1 to 15 Å), meaning that the titanate is a lepidocrocite-type structure having relaxed atom positions within the restraints. It is apparent that the Ti positions are disordered (Figure 6c). Thus, we consider that this disordered prestructure of the lepidocrocite grows to form larger 2D lepidocrocite structures upon thermal treatment.

CONCLUSIONS

This work has revealed that (i) titanium isopropoxide forms segregated tiny cluster-like or disordered corrugated lepidocrocite-type structures with <7 Å domains in alkaline aqueous solution (pH = 14), (ii) these prestructures directly form lepidocrocite-layered titanate without forming intermediates upon thermal treatment (as shown in Figure 7), (iii) the structural transformation commences immediately after starting the thermal treatment, (iv) further treatment results in gradual growth of the layers and their stacking commences, and (v) the layered structure dispersed in the solution is slightly different from that in crystals having interlayer TMAH. Thus, we conclude that the formation of the lepidocrocite-like prestructure is the key for forming the layered titanate under hydrothermal conditions.

MATERIALS AND METHODS

Design of in Situ X-ray Measurements. We have developed a system, in which hydrothermal/solvothermal reactions are monitored by in situ X-ray scattering as well as a pressure sensor and a temperature sensor (Figure S5). The

DOI: 10.1021/acsomega.8b01693
ACS Omega 2018, 3, 8874−8881

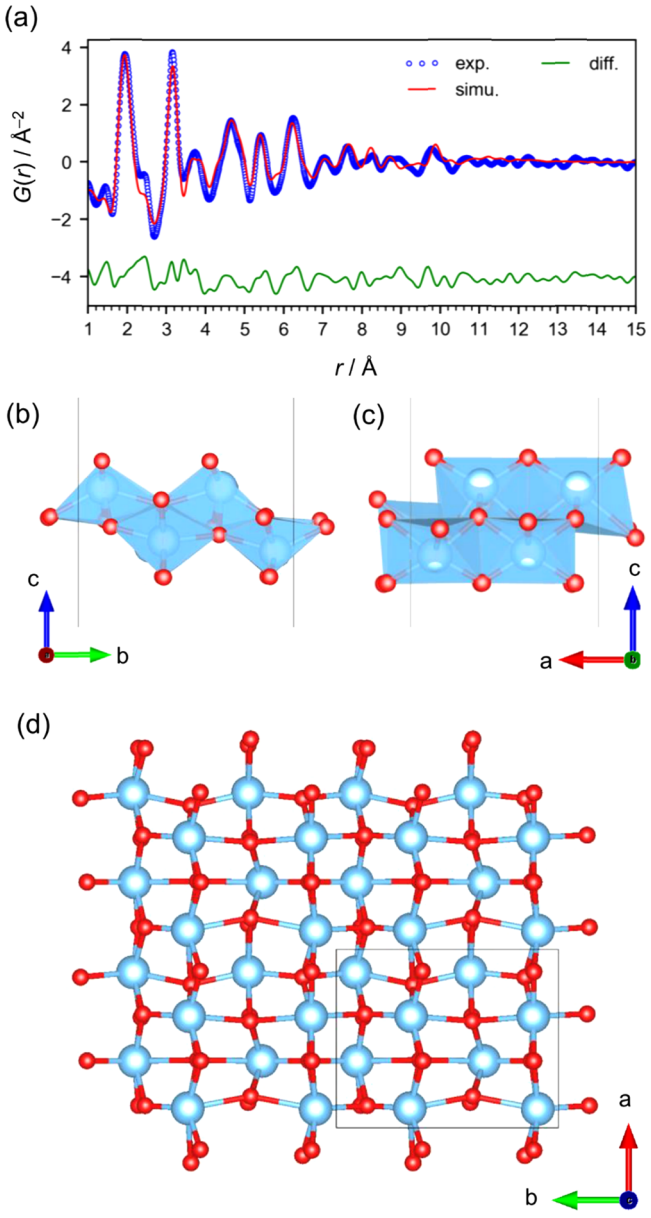

Figure 6. (a) PDF curve-fitting result for the titanate in the as-prepared solution measured at RT. (b–d) Lepidocrocite-type layered titanate structure model (2 × 2 × 1 supercell in *P*1 space group).

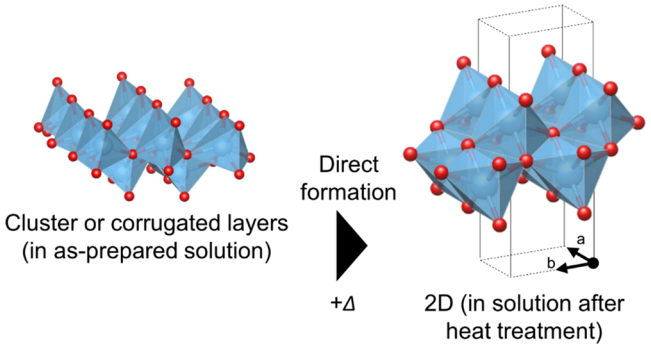

Figure 7. Summary of the hydrothermal reaction of titanium isopropoxide at pH 14. The as-mixed solution contains clusters or corrugated layers of lepidocrocite-like networks. Upon heating, the lepidocrocite-like domains become ordered and grow.

penetration of X-ray was ensured by using synchrotron high-energy X-rays (115 keV), sufficient time resolution was obtained using a flat panel detector, and a good signal-to-noise ratio was ensured by developing a data-processing program. The apparatus was designed on the basis of the criteria for successful in situ diffraction measurements under the hydrothermal conditions summarized by Walton and O'Hare, in brief, (i) a good signal-to-noise ratio (or high intensity of Bragg peaks relative to the diffuse scattering), (ii) the sufficient penetration of X-rays through containers, and (iii) sufficient time resolution to discuss the kinetics.[33]

Microwave Synthesis. The chemical reactions were carried out under hydrothermal conditions using a Biotage Initiator microwave reactor. Five milliliters of solution was placed in a dedicated glass vial (2–5 mL). We chose microwave heating because it directly heats the solvent (not through thermal conduction), that is, reactions are considered to proceed homogeneously. The reactor was modified by forming holes in the metallic compartment and removing the Teflon inner walls to allow X-rays to pass through the glass vial with the minimum background intensity associated with the reactor. The temperature of the solution ∼1 cm below the liquid level was monitored by an infrared sensor, whereas the solution ∼1.5 cm above the bottom was irradiated by X-rays. The solution was mixed with a magnetic stir bar at 600 rpm. Note that this operation requires careful calibration of the system. The temperature and pressure in the vial were monitored using the sensors of the reactor, and the color of the liquid was monitored using a camera. We investigated whether the structures of the final products are identical in the microwave heating experiments and conventional heating using autoclaves through ex situ XRD experiments.

Chemicals. Titanium isopropoxide (0.67 g) was mixed in 6.68 mL of TMAH (12.5%, Nacalai Tesque; diluted with pure water) in the glass vial of the microwave reactor. The pH value was constant at 14.0 before and after the microwave reactions. For the preparation of the dry product, the titanate was precipitated by adding isopropanol into the solution, filtered, rinsed with isopropanol, and then dried.

Elemental Analysis. Elemental analysis was performed using a Hitachi SPS3520UV-DD inductively coupled plasma optical emission spectrometer for Ti, using a LECO TC436 elemental analyzer for O in oxides and using a LECO CS-444LS analyzer for C. The obtained contents were Ti (44.0 wt %), O (34 ± 1 wt %), C (10.4 ± 0.2 wt %), and N (1.5 ± 0.1 wt %). Note that these measurements reflect the composition of nonvolatile components, giving the Ti to O atomic ratio of Ti/O = 1.00:1.99. Because this measurement of the N content is less reliable than those of the other elements, we performed a CHN analysis using a PerkinElmer PE2400II instrument and obtained contents of C (10.0 wt %), H (3.4 wt %), and N (2.8 wt %), giving a molar ratio of $C_{0.83}H_{3.4}N_{0.20}$. The composition was thus determined as $[TiO_2]\cdot nH_2O\cdot m((CH_3)_4N)$ (n = 0.54 and m = 0.22). The content of TMAH was constant even after purification through the recrystallization process.

In Situ PDF Measurements. A rapid-acquisition pair distribution function analysis was carried out at the BL08W beamline in SPring-8. The X-ray scattering data were collected on a PerkinElmer flat panel detector using monochromated X-rays at 115 keV. The data were recorded every 1 min by averaging 60 frames of image data collected with an exposure of 1.0 s per frame. The optics, including the beam center coordinates, the tilt of the detector, and the sample-to-detector

DOI: 10.1021/acsomega.8b01693
ACS Omega 2018, 3, 8874–8881

distance, were calibrated using image data obtained for CeO_2 (NIST 674B) packed in a Kapton capillary (ϕ 1 mm) fixed at the center of the glass vial loaded in the microwave reactor.

The data for the solvent only (Figure S6) were obtained for a solution prepared by adding titanium isopropoxide to pure water, extracting the liquid phase, and then adding TMAH solution to the solution. This solution contains water, TMAH, and isopropanol at the same concentrations as those in the titanate solution used for the hydrothermal synthesis.

Ex Situ X-ray Measurements. X-ray total scattering data were collected on a Rigaku RAXIS-IV imaging plate detector at the BL10XU beamline in SPring-8 (λ = 0.19909 Å, determined using CeO_2). The exposure time was 600 s. The sample was packed in a Kapton capillary (ϕ 1 mm). After roughly determining the structure using this PDF data (Q_{max} = 20.0 $Å^{-1}$), further analysis was performed using the data collected at the BL08W beamline in SPring-8 (λ = 0.1076 Å, Q_{max} = 29.0 $Å^{-1}$). In addition to these PDF data, synchrotron XRD data were collected using PILATUS 100K semiconductor detectors at the BL5S2 beamline (beam size = 0.5 mm × 0.5 mm, λ = 1.29945 Å) at 25 °C. The crystal structure was determined using the EXPO2014 program.

Data Processing. We used the PIXIA program to convert image data to one-dimensional profiles through mathematical noise filtration and calculations based on X-ray scattering physics (details are available in the Supporting Information; the program was developed as part of the Orochi Project and will be available from the National Institute for Materials Science).[34] This is because the resolution of in situ and/or time-resolved measurements is likely to get worse than the ex situ resolution owing to the lower signal-to-noise ratio, and it may not be possible to monitor the trace of a structural change, which is likely hidden by noise. Details are available in the Supporting Information (Figures S12−S17 and related explanations).

To monitor the structural changes during synchrotron measurements, we used an extended concept of differential PDFs, referred to as "relative PDFs", to detect even faint changes associated with the structural transformation in the nucleation stage. These relative PDFs are useful for monitoring structural changes during the measurements. The differential PDFs are the pair correlation functions between all atoms and a particular chemical species[22] and are used to discuss changes in the chemical species of interest. They are obtained by calculation of the difference between two sets of total scattering data or PDFs that are measured at different concentrations or the scattering factors of particular chemical species.[22,35−37]

In contrast to these intended and selective modulations, it is difficult to know the changes in the chemical species in reactions in advance, and thus accurate differential PDFs cannot be obtained. However, we consider that a simple calculation of the relative values of PDFs (details are available in the Supporting Information) from the total scattering data is useful for detecting a trace of a structural change even without accurate normalization using scattering factors for the chemical species assumed to change in the reactions. These relative PDFs are basically similar to differential PDFs and are easily calculated with minimal noise to monitor the reactions during total scattering experiments, although the amplitude may be less meaningful owing to the normalization. Considering the fact that the normalization in extended X-ray absorption fine structures (EXAFS) is often based on a spline function, the normalization for the relative PDFs is acceptable.

Other Measurements. Simultaneous thermogravimetric analysis and differential thermal analysis (TG-DTA) were performed using a Hitachi HT-Seiko Instrument Exter 6300 instrument (5 °C min^{-1}, RT to 600 °C in air). Fourier transform infrared spectroscopy was carried out using a Thermo Fisher Scientific Nicolet 4700 spectrometer in the transmission mode (KBr pellets).

■ ASSOCIATED CONTENT

Supporting Information

The Supporting Information is available free of charge on the ACS Publications website at DOI: 10.1021/acsomega.8b01693.

TG-DTA, Fourier transform infrared, overview of in situ experiments, total scattering data with and without titanate, photographs of solution, details of PDF curve fitting, theoretical details of data processing, structure information obtained by curve fitting (PDF)

■ AUTHOR INFORMATION

Corresponding Author

*E-mail: TOMINAKA.Satoshi@nims.go.jp.

ORCID

Satoshi Tominaka: 0000-0001-6474-8665

Notes

The authors declare no competing financial interest.

■ ACKNOWLEDGMENTS

This work was partly supported by the World Premier International Research Center (WPI) Initiative on Materials Nanoarchitectonics from MEXT, Japan, and by a Grant-in-Aid for Scientific Research C (18K05192) from JSPS, Japan. The synchrotron radiation experiments were performed at BL08W (in situ) and BL10XU (ex situ) of SPring-8 with the approval of the Japan Synchrotron Radiation Research Institute (JASRI) (Proposal Nos. 2017A1207 and 2016B1954). We thank Dr. H. Nara (Waseda Univ.) for the help in the CHN analysis, A. Salman (NIMS) for the help in the TGA measurements, K. Iiyama (NIMS) for the experimental support, and N. Tsuji and K. Nakada (JASRI) for the help in the synchrotron measurements.

■ REFERENCES

(1) Gateshki, M.; Yin, S.; Ren, Y.; Petkov, V. Titania polymorphs by soft chemistry: Is there a common structural pattern? *Chem. Mater.* **2007**, *19*, 2512−2518.

(2) Ma, J.; Reeves, K. G.; Gutierrez, A. G. P.; Body, M.; Legein, C.; Kakinuma, K.; Borkiewicz, O. J.; Chapman, K. W.; Groult, H.; Salanne, M.; Dambournet, D. Layered Lepidocrocite Type Structure Isolated by Revisiting the Sol-Gel Chemistry of Anatase TiO_2: A New Anode Material for Batteries. *Chem. Mater.* **2017**, *29*, 8313−8324.

(3) Tominaka, S.; Ishihara, A.; Nagai, T.; Ota, K.-i. Noncrystalline Titanium Oxide Catalysts for Electrochemical Oxygen Reduction Reactions. *ACS Omega* **2017**, *2*, 5209−5214.

(4) Mi, J. L.; Jensen, K. M. O.; Tyrsted, C.; Bremholm, M.; Iversen, B. B. In situ total X-ray scattering study of the formation mechanism and structural defects in anatase TiO_2 nanoparticles under hydrothermal conditions. *CrystEngComm* **2015**, *17*, 6868−6877.

(5) Karthika, S.; Radhakrishnan, T. K.; Kalaichelvi, P. A Review of Classical and Nonclassical Nucleation Theories. *Cryst. Growth Des.* **2016**, *16*, 6663−6681.

DOI: 10.1021/acsomega.8b01693
ACS Omega 2018, 3, 8874−8881

(6) Bøjesen, E. D.; Iversen, B. B. The chemistry of nucleation. *CrystEngComm* **2016**, *18*, 8332−8353.
(7) Giessen, B. C.; Gordon, G. E. X-Ray Diffraction - New High-Speed Technique Based on X-Ray Spectrography. *Science* **1968**, *159*, 973−975.
(8) Francis, R. J.; O'Brien, S.; Fogg, A. M.; Halasyamani, P. S.; O'Hare, D.; Loiseau, T.; Ferey, G. Time-resolved in-situ energy and angular dispersive X-ray diffraction studies of the formation of the microporous gallophosphate ULM-5 under hydrothermal conditions. *J. Am. Chem. Soc.* **1999**, *121*, 1002−1015.
(9) Barnes, P.; Clark, S. M.; Häusermann, D.; Henderson, E.; Fentiman, C. H.; Muhamad, M. N.; Rashid, S. Time-resolved studies of the early hydration of cements using synchrontron energy-dispersive diffraction. *Phase Transitions* **1992**, *39*, 1−4.
(10) Christensen, A. N.; Jensen, T. R.; Norby, P.; Hanson, J. C. In situ synchrotron x-ray powder diffraction studies of crystallization of microporous aluminophosphates and Me^{2+}-substituted aluminophosphates. *Chem. Mater.* **1998**, *10*, 1688−1693.
(11) Norby, P. Hydrothermal conversion of zeolites: An in situ synchrotron X-ray powder diffraction study. *J. Am. Chem. Soc.* **1997**, *119*, 5215−5221.
(12) Bremholm, M.; Felicissimo, M.; Iversen, B. B. Time-Resolved In Situ Synchrotron X-ray Study and Large-Scale Production of Magnetite Nanoparticles in Supercritical Water. *Angew. Chem., Int. Ed.* **2009**, *48*, 4788−4791.
(13) Dalod, A. R. M.; Grendal, O. G.; Skjaervo, S. L.; Inzani, K.; Selbach, S. M.; Henriksen, L.; van Beek, W.; Grande, T.; Einarsrud, M. A. Controlling Oriented Attachment and in Situ Functionalization of TiO_2 Nanoparticles During Hydrothermal Synthesis with APTES. *J. Phys. Chem. C* **2017**, *121*, 11897−11906.
(14) Saito, K.; Tominaka, S.; Yoshihara, S.; Ohara, K.; Sugahara, Y.; Ide, Y. Room-Temperature Rutile TiO_2 Nanoparticle Formation on Protonated Layered Titanate for High-Performance Heterojunction Creation. *ACS Appl. Mater. Interfaces* **2017**, *9*, 24538−24544.
(15) Jensen, K. M. O.; Christensen, M.; Juhas, P.; Tyrsted, C.; Bojesen, E. D.; Lock, N.; Billinge, S. J. L.; Iversen, B. B. Revealing the Mechanisms behind SnO_2 Nanoparticle Formation and Growth during Hydrothermal Synthesis: An In Situ Total Scattering Study. *J. Am. Chem. Soc.* **2012**, *134*, 6785−6792.
(16) Zhang, F.; Chupas, P. J.; Lui, S. L. A.; Hanson, J. C.; Caliebe, W. A.; Lee, P. L.; Chan, S. W. In situ study of the crystallization from amorphous to cubic zirconium oxide: Rietveld and reverse Monte Carlo analyses. *Chem. Mater.* **2007**, *19*, 3118−3126.
(17) Jensen, K. M. Ø.; Tyrsted, C.; Bremholm, M.; Iversen, B. B. In Situ Studies of Solvothermal Synthesis of Energy Materials. *ChemSusChem* **2014**, *7*, 1594−1611.
(18) Nielsen, M. H.; Aloni, S.; De Yoreo, J. J. In situ TEM imaging of $CaCO_3$ nucleation reveals coexistence of direct and indirect pathways. *Science* **2014**, *345*, 1158−1162.
(19) Liao, H. G.; Zherebetskyy, D.; Xin, H. L.; Czarnik, C.; Ercius, P.; Elmlund, H.; Pan, M.; Wang, L. W.; Zheng, H. M. Facet development during platinum nanocube growth. *Science* **2014**, *345*, 916−919.
(20) Walton, R. I.; Millange, F.; O'Hare, D.; Davies, A. T.; Sankar, G.; Catlow, C. R. A. An in situ energy-dispersive X-ray diffraction study of the hydrothermal crystallization of zeolite A. 1. Influence of reaction conditions and transformation into sodalite. *J. Phys. Chem. B* **2001**, *105*, 83−90.
(21) Engelke, L.; Schaefer, M.; Schur, M.; Bensch, W. In situ X-ray diffraction studies of the crystallization of layered manganese thioantimonates(III) under hydrothermal conditions. *Chem. Mater.* **2001**, *13*, 1383−1390.
(22) Egami, T.; Billinge, S. J. L. *Underneath the Bragg Peaks: Structural Analysis of Complex Materials*; Elsevier: Oxford, U.K., 2003.
(23) Chupas, P. J.; Chaudhuri, S.; Hanson, J. C.; Qiu, X. Y.; Lee, P. L.; Shastri, S. D.; Billinge, S. J. L.; Grey, C. P. Probing local and long-range structure simultaneously: An in situ study of the high-temperature phase transition of alpha-AlF_3. *J. Am. Chem. Soc.* **2004**, *126*, 4756−4757.
(24) Sasaki, T.; Watanabe, M.; Michiue, Y.; Komatsu, Y.; Izumi, F.; Takenouchi, S. Preparation and Acid-Base Properties of a Protonated Titanate with the Lepidocrocite-Like Layer Structure. *Chem. Mater.* **1995**, *7*, 1001−1007.
(25) Groult, D.; Mercey, C.; Raveau, B. New Oxides with Layer Structure - Nonstoichiometric Potassium Titanate $K_x(M_yTi_{2-y})O_4$. *J. Solid State Chem.* **1980**, *32*, 289−296.
(26) Altomare, A.; Cuocci, C.; Giacovazzo, C.; Moliterni, A.; Rizzi, R.; Corriero, N.; Falcicchio, A. EXPO2013: a kit of tools for phasing crystal structures from powder data. *J. Appl. Crystallogr.* **2013**, *46*, 1231−1235.
(27) Sato, H.; Ono, K.; Sasaki, T.; Yamagishi, A. First-principles study of two-dimensional titanium dioxides. *J. Phys. Chem. B* **2003**, *107*, 9824−9828.
(28) Farrow, C. L.; Juhas, P.; Liu, J. W.; Bryndin, D.; Bozin, E. S.; Bloch, J.; Proffen, T.; Billinge, S. J. L. PDFfit2 and PDFgui: computer programs for studying nanostructure in crystals. *J. Phys.: Condens. Matter* **2007**, *19*, No. 335219.
(29) Zobel, M.; Neder, R. B.; Kimber, S. A. J. Universal solvent restructuring induced by colloidal nanoparticles. *Science* **2015**, *347*, 292−294.
(30) Dodd, D.; Hardcastle, F. D.; Laffoon, S. Titanium-Oxygen Bond Length-Bond Valence Relationship. *J. Arkansas Acad. Sci.* **2013**, *67*, 42−45.
(31) Gong, Y.; Zhou, M. F. Matrix infrared spectra and density functional calculations of TiO3 and TiO5 in solid argon. *J. Phys. Chem. A* **2008**, *112*, 9758−9762.
(32) Tominaka, S.; Kawakami, K.; Fukushima, M.; Miyazaki, A. Physical Stabilization of Pharmaceutical Glasses Based on Hydrogen Bond Reorganization under Sub-T_g Temperature. *Mol. Pharmaceutics* **2017**, *14*, 264−273.
(33) Walton, R. I.; O'Hare, D. Watching solids crystallise using in situ powder diffraction. *Chem. Commun.* **2000**, *23*, 2283−2291.
(34) National Institute for Materials Science. Samurai System for Satoshi Tominaka, 2018, https://samurai.nims.go.jp/profiles/tominaka_satoshi (accessed July 17, 2018).
(35) Chapman, K. W.; Chupas, P. J.; Kepert, C. J. Selective recovery of dynamic guest structure, in a nanoporous Prussian blue through in situ X-ray diffraction: A differential pair distribution function analysis. *J. Am. Chem. Soc.* **2005**, *127*, 11232−11233.
(36) Chupas, P. J.; Chapman, K. W.; Jennings, G.; Lee, P. L.; Grey, C. P. Watching nanoparticles grow: The mechanism and kinetics for the formation of TiO_2-supported platinum nanoparticles. *J. Am. Chem. Soc.* **2007**, *129*, 13822−13824.
(37) Shiotani, S.; Ohara, K.; Tsukasaki, H.; Mori, S.; Kanno, R. Pair distribution function analysis of sulfide glassy electrolytes for all-solid-state batteries: Understanding the improvement of ionic conductivity under annealing condition. *Sci. Rep.* **2017**, *7*, No. 6972.

DOI: 10.1021/acsomega.8b01693
ACS Omega 2018, 3, 8874−8881